Physics Letters B 668 (2008) 44–50

Contents lists available at ScienceDirect

Physics Letters B

www.elsevier.com/locate/physletb

# Stochastic backgrounds of relic gravitons, TΛCDM paradigm and the stiff ages

Massimo Giovannini [a,b,*]

[a] Department of Physics, Theory Division, CERN, 1211 Geneva 23, Switzerland
[b] INFN, Section of Milan-Bicocca, 20126 Milan, Italy

ARTICLE INFO

*Article history:*
Received 11 July 2008
Accepted 30 July 2008
Available online 12 August 2008
Editor: L. Alvarez-Gaumé

ABSTRACT

Absent any indirect tests on the thermal history of the Universe prior to the formation of light nuclear elements, it is legitimate to investigate situations where, before nucleosynthesis, the sound speed of the plasma was larger than $c/\sqrt{3}$, at most equalling the speed of light $c$. In this plausible extension of the current cosmological paradigm, hereby dubbed Tensor-ΛCDM (i.e. TΛCDM) scenario, high-frequency gravitons are copiously produced. Without conflicting with the bounds on the tensor to scalar ratio stemming from the combined analysis of the three standard cosmological data sets (i.e. cosmic microwave background anisotropies, large-scale structure and supenovae), the spectral energy density of the relic gravitons in the TΛCDM scenario can be potentially observable by wide-band interferometers (in their advanced version) operating in a frequency window which ranges between few Hz and few kHz.



The only direct informations on the early thermal history of the Universe come, at present, from a background of relic photons which last scattered the electrons at an approximate redshift of $z_{\rm dec} \simeq 1087$ according to the 5-yr WMAP data release [1,2]. The scrutiny of the Cosmic Microwave Background (CMB) observables is always conducted within a commonly accepted framework, i.e. the so-called ΛCDM paradigm where Λ qualifies the dark-energy component (parametrized in terms of a cosmological constant) and CDM qualifies the (cold) dark matter component. The ΛCDM scenario represents a useful compromise between the available data and the number of ascertainable parameters. A class of plausible completions of the ΛCDM model contemplates the addition of a post-inflationary phase expanding at a rate which is slower than radiation. From the point of view of the fluid properties, the sources generating such a dynamics are often called stiff. The spectral energy density of the gravitons reentering the Hubble radius during the stiff phase increases with the frequency rather than being nearly constant as in the conventional ΛCDM paradigm. Such an extension requires two parameters: a typical frequency scale, be it $\nu_{\rm s}$ (corresponding to the end of the stiff epoch) and the slope of the spectral energy density during the stiff phase. The supplementary parameters characterizing this scenario (which will be dubbed, in what follows, as TΛCDM for tensor-ΛCDM) can be determined by analyzing the three conventional cosmological data sets (i.e. CMB [1,2], large-scale structure [3,4] and supernovae [5,6]) in conjunction with the forthcoming data of wide-band interferometers [7–10]. At the moment interferometers are only able to provide interesting upper limits on the spectral energy density of the relic gravitons [11]. The foreseen sensitivities of the so-called advanced Ligo [7] will still be inadequate to probe the relic gravitons produced within the conventional ΛCDM scenario. Nonetheless the very same sensitivities of the interferometers in their advanced version will be definitely sufficient to probe directly the parameter space of the TΛCDM scenario.

Consider therefore the evolution of the tensor modes in conformally flat background geometries which are, incidentally, the ones currently preferred in the context of the ΛCDM paradigm [1,2]. A conformally flat background geometry in four space–time dimensions, by definition, is characterized by a metric $\bar{g}_{\mu\nu} = a^2(\tau)\eta_{\mu\nu}$ where $\eta_{\mu\nu}$ is the Minkowski metric with signature mostly minus and $\tau$ is the so-called conformal time coordinate. The tensor fluctuations of the geometry are defined with respect to the three-dimensional Euclidean sub-manifold as

$$\delta^{(1)}_{\rm t} g_{ij} = -a^2 h_{ij}, \qquad \delta^{(1)}_{\rm t} g^{ij} = \frac{h^{ij}}{a^2},$$
$$\delta^{(2)}_{\rm t} g^{ij} = -\frac{h^i_k h^{kj}}{a^2}, \qquad \partial_i h^i_j = h^i_i = 0, \tag{1}$$

where Latin indices run over the spatial dimensions; $\delta^{(1)}_{\rm t}$ and $\delta^{(2)}_{\rm t}$ denote, respectively, the first and second order tensor fluctuations of the corresponding quantity. Since $h_{ij}$ is a (divergenceless and traceless) rank-two tensor in three spatial dimensions, it carries two physical polarizations. Defining three mutually orthogonal directions as $\hat{k}_i = k_i/|\vec{k}|$, $\hat{m}_i = m_i/|\vec{m}|$ and $\hat{n}_i = n_i/|\vec{n}|$, the two polarizations of the gravitons in a conformally flat background are nothing but

* Correspondence address: Department of Physics, Theory Division, CERN, 1211 Geneva 23, Switzerland.
*E-mail address:* massimo.giovannini@cern.ch.

0370-2693 
doi:10.1016/j.physletb.2008.07.107

$$\epsilon_{ij}^{(\oplus)}(\hat{k}) = (\hat{m}_i\hat{m}_j - \hat{n}_i\hat{n}_j), \qquad \epsilon_{ij}^{(\otimes)}(\hat{k}) = (\hat{m}_i\hat{n}_j + \hat{n}_i\hat{m}_j),$$
$$\epsilon_{ij}^{(\lambda)}\epsilon_{ij}^{(\lambda')} = 2\delta_{\lambda\lambda'}. \tag{2}$$

By perturbing the Einstein–Hilbert action to second order in the tensor amplitude $h_{ij}$, the action for the gravitons can be written, up to total derivatives, as

$$S_{\rm gw} = \delta_{\rm t}^{(2)} S = \frac{1}{8\ell_{\rm P}^2}\int d^4x\sqrt{-\bar{g}}\bar{g}^{\mu\nu}\partial_\mu h_{ij}\partial_\nu h^{ij},$$
$$\ell_{\rm P} = \sqrt{8\pi G} = \frac{8\pi}{M_{\rm P}} = \frac{1}{\bar{M}_{\rm P}}. \tag{3}$$

Up to a rescaling of the amplitude in terms of the Planck length, the canonical normal modes of the action (3) are given by $\mu_{ij} = a h_{ij}$ since, in a conformally flat background, $\sqrt{-\bar{g}}\bar{g}^{\mu\nu} \to a^2(\tau)\eta^{\mu\nu}$. The mode expansion of the canonical field operator is thus given by:

$$\hat{\mu}_{ij}(\vec{x},\tau) = \frac{\sqrt{2}\ell_{\rm P}}{(2\pi)^{3/2}} \times \sum_\lambda \int d^3k\, \epsilon_{ij}^{(\lambda)}(\hat{k})\left[\hat{a}_{\vec{k},\lambda} f_{k,\lambda}(\tau) e^{-i\vec{k}\cdot\vec{x}} + \hat{a}^\dagger_{\vec{k},\lambda} f^*_{k,\lambda}(\tau) e^{i\vec{k}\cdot\vec{x}}\right], \tag{4}$$

where $[\hat{a}_{\vec{k},\lambda}, \hat{a}^\dagger_{\vec{p},\lambda'}] = \delta^{(3)}(\vec{k}-\vec{p})\delta_{\lambda\lambda'}$. It will be hereby assumed that the field operators are in the vacuum at the onset of the inflationary evolution. Thus the initial state $|0\rangle$ (annihilated by $\hat{a}_{\vec{k},\lambda}$) minimizes the tensor Hamiltonian when all the wavelengths of the field are shorter than the event horizon at the onset of the inflationary evolution (see, for instance, [12]). In Eq. (4) $f_{k,\lambda}$ are the (complex) tensor mode functions obeying

$$f'_{k,\lambda} = g_{k,\lambda}, \qquad g'_{k,\lambda} = -\left[k^2 - \left(\mathcal{H}' + \mathcal{H}^2\right)\right] f_{k,\lambda}, \quad \mathcal{H} = \frac{a'}{a}, \tag{5}$$

where the prime denotes a derivation with respect to the conformal time coordinate $\tau$. Defining $p_{\rm t}$ and $\rho_{\rm t}$ as the total pressure and as the total energy density of the plasma, the Friedmann–Lemaître equations read:

$$\mathcal{H}^2 = \frac{8\pi G}{3}a^2\rho_{\rm t}, \qquad \mathcal{H}^2 - \mathcal{H}' = 4\pi G a^2(\rho_{\rm t} + p_{\rm t}),$$
$$\rho'_{\rm t} + 3\mathcal{H}(\rho_{\rm t} + p_{\rm t}) = 0. \tag{6}$$

If the inflationary phase is suddenly followed by the radiation-dominated phase, the energy density of the inflaton is instantaneously converted into a radiation. This approximation is customarily employed to assess the number of inflationary e-folds [12,13]. Given our ignorance on the thermal history of the plasma prior to nucleosynthesis, the inflationary phase might not be suddenly followed by the radiation dominated phase [14,15]. Provided the transition between inflation and radiation is sufficiently stiff (and long) high-frequency gravitons can be copiously produced [14,15]. A relativistic plasma is said to be stiff if its sound speed is larger than the sound speed of a gas of ultra-relativistic particles[1] i.e. $1/\sqrt{3}$. The total sound speed and the barotropic index are defined, respectively, as:

$$c_{\rm st}^2 = \frac{\partial p_{\rm t}}{\partial \rho_{\rm t}} = w_{\rm t} - \frac{1}{3}\frac{\partial(w_{\rm t}+1)}{\partial \ln a}, \quad w_{\rm t} = \frac{p_{\rm t}}{\rho_{\rm t}}, \tag{7}$$

where, in the second equality defining $c_{\rm st}^2$, Eq. (6) has been used. In the primeval plasma, stiff phases can arise: this idea goes back to the pioneering suggestions of Zeldovich [16] in connection with the entropy problem. If an inflationary phase precedes a stiff phase the spectral energy density of the relic gravitons increases with frequency and the typical length of the stiff epoch can be determined by back-reaction effects [14]. In [15] the techniques of [14] were applied to assess the spectral energy density in the models of quintessential inflation which were developed in [17]. There were various reprises of these ideas (see, for instance, [18] and references therein). A (causal) upper limit on $w_{\rm t}$ and $c_{\rm st}$ is the speed of light, i.e. $w_{\rm t} \leqslant c_{\rm st} \leqslant 1$ [19].

Collisionless species couple to the tensor modes of the geometry. Defining as $\Pi_{ij}$ the anisotropic stress of the plasma we will actually have that below temperatures $\mathcal{O}$(MeV), i.e. after weak interactions fall out of thermal equilibrium, the evolution equations for the classical amplitude corresponding to the quantum operators of Eq. (4) reads

$$\mu''_{ij} - \nabla^2\mu_{ij} - \left(\mathcal{H}' + \mathcal{H}^2\right)\mu_{ij} = -16\pi G a^3 \Pi_{ij}. \tag{8}$$

The coupling to the anisotropic stress induces computable differences on the spectral energy density of the relic gravitons. The effects of neutrino free streaming has been investigated both semi-analytically and numerically in [20] (see also [21–23]). With this caveat on collisionless species, Eqs. (5) and (6) can be solved numerically; the spectral energy density of the relic gravitons (and the related power spectrum) can then be assessed.

The definition of the energy–momentum pseudo-tensor of the gravitational field always involves a certain degree of ambiguity. After getting rid of the tensor structure by making explicit the two physical polarizations, the action of Eq. (3) is just the action of two minimally coupled scalar fields in a conformally flat geometry of Friedmann–Robertson–Walker (FRW) type. The energy–momentum pseudo-tensor of relic gravitons in a FRW background just given by [24]

$$T_\mu^\nu = \frac{1}{4\ell_{\rm P}^2}\left[\partial_\mu h_{ij}\partial^\nu h^{ij} - \frac{1}{2}\delta_\mu^\nu \bar{g}^{\alpha\beta}\partial_\alpha h_{ij}\partial_\beta h^{ij}\right]$$
$$= \frac{1}{2\ell_{\rm P}^2}\sum_\lambda\left[\partial_\mu h_{(\lambda)}\partial^\nu h^{(\lambda)} - \frac{1}{2}\bar{g}^{\alpha\beta}\partial_\alpha h_{(\lambda)}\partial_\beta h_{(\lambda)}\delta_\mu^\nu\right], \tag{9}$$

where the second equality follows from the first by using $h_{ij} = \sum_\lambda h_{(\lambda)}\epsilon_{ij}^\lambda$ and by recalling the orthogonality condition appearing in Eq. (2). In a complementary perspective [25], the energy–momentum pseudo-tensor is instead defined from the second-order fluctuations of the Einstein tensor, i.e.

$$\mathcal{T}_\mu^\nu = -\frac{1}{\ell_{\rm P}^2}\delta_{\rm t}^{(2)}\mathcal{G}_\mu^\nu, \quad \mathcal{G}_\mu^\nu = R_\mu^\nu - \frac{1}{2}\delta_\mu^\nu R, \tag{10}$$

where the superscript at the right-hand side denotes the second-order fluctuation of the corresponding quantity while the subscript refers to the tensor nature of the fluctuations. The two definitions seem very different but the energy densities and pressures derived in the two approaches give coincident results as soon as the corresponding wavelengths are inside the Hubble radius, i.e. $k > \mathcal{H}$. In the opposite limit Eqs. (9) and (10) seem superficially different but give consistent quantitative results once they are compared on a particular background geometry [26].

By definition, $\rho_{\rm GW}(\vec{x},\tau) = \langle 0|T_0^0(\vec{x},\tau)|0\rangle$ where $|0\rangle$ is, again, the state annihilated by $a_{k,\lambda}$. Recalling that the mode functions of each polarization coincide (i.e., in Eq. (5), $f_{k,\oplus} = f_{k,\otimes} = f_k$ and analogously for $g_k$) the spectral energy density in critical units can then be expressed as:

$$\Omega_{\rm GW}(k,\tau) = \frac{1}{\rho_{\rm crit}}\frac{d\rho_{\rm GW}}{d\ln k} = \frac{k^3}{2\pi^2 a^4\rho_{\rm crit}}\Delta_\rho(k,\tau),$$
$$\rho_{\rm crit} = \frac{3H^2}{8\pi G} = 3\bar{M}_{\rm P}^2 H^2,$$

[1] Natural units $\hbar = c = k_{\rm B} = 1$ are used throughout the Letter.

$$\Delta_\rho(k,\tau) = \bigl\{\bigl|g_k(\tau)\bigr|^2 + \bigl(k^2+\mathcal{H}^2\bigr)\bigl|f_k(\tau)\bigr|^2 - \mathcal{H}\bigl[f_k^*(\tau)g_k(\tau) + f_k(\tau)g_k^*(\tau)\bigr]\bigr\}. \tag{11}$$

The spectral energy density of the relic gravitons can be related to the power spectrum which is, by definition, the Fourier transform of the two-point function evaluated at equal times, i.e. using Eq. (4)

$$\langle 0|\hat{h}_{ij}(\vec{x},\tau)\hat{h}^{ij}(\vec{y},\tau)|0\rangle = \int d\ln k\, \mathcal{P}_{\rm T}(k,\tau)\frac{\sin kr}{kr},$$
$$\mathcal{P}_{\rm T}(k,\tau) = 4\ell_{\rm P}^2\frac{k^3}{\pi^2 a^2(\tau)}\bigl|f_k(\tau)\bigr|^2, \tag{12}$$

where $r = |\vec{x}-\vec{y}|$. Quantum fluctuations present during the inflationary phase are amplified with nearly scale-invariant slope. The inflationary power spectra are then parametrized in terms of the tensor and scalar spectral indices, i.e., respectively, $n_{\rm T}$ and $n_{\rm s}$:

$$r_{\rm T} = \frac{\mathcal{A}_{\rm T}}{\mathcal{A}_{\mathcal{R}}},$$
$$\bar{\mathcal{P}}_{\rm T}(k) = \mathcal{A}_{\rm T}\left(\frac{k}{k_{\rm p}}\right)^{n_{\rm T}}, \qquad \bar{\mathcal{P}}_{\mathcal{R}}(k) = \mathcal{A}_{\mathcal{R}}\left(\frac{k}{k_{\rm p}}\right)^{n_{\rm s}-1}, \tag{13}$$

where $k_{\rm p} = 0.002\ {\rm Mpc}^{-1}$ is the so-called pivot wave-number which corresponds to an effective multipole $\ell_{\rm eff} \simeq 30$. In the context of the $\Lambda$CDM paradigm, the 5-yr WMAP data alone imply $\mathcal{A}_{\mathcal{R}} = 2.41\times 10^{-9}$ (slightly different values can be obtained if different data sets are combined but these differences do not affect the features addressed here). The tensor amplitude is therefore estimated by setting limits on $r_{\rm T}$ which is, by definition, the ratio between the tensor and the scalar amplitudes evaluated at the pivot scale $k_{\rm p}$. The inferred upper bounds on $r_{\rm T}$, range from $r_{\rm T} < 0.2$ (in the case of the WMAP 5-yr data alone [1,2]) up to $r_{\rm T} < 0.43$ when the WMAP 5-yr data are combined with the large-scale [3,4] and supernova data [5,6] (see also the thorough analyses reported in [1,2]). In the minimal version of the inflationary dynamics the tensor spectral slope (i.e. $n_{\rm T}$), the slow roll parameter $\epsilon$ as well as $r_{\rm T}$ are all related:

$$n_{\rm T} \simeq -\frac{r_{\rm T}}{8} \simeq -2\epsilon, \quad \epsilon = -\frac{\dot{H}}{H^2} > 0, \tag{14}$$

where $\epsilon$ measures, as indicated, the (slight) decrease of the Hubble $H$ rate during the quasi-de Sitter phase of expansion and the overdot in the last equation denotes a derivation with respect to the cosmic time coordinate. Usually Eq. (12) is computed at the present epoch and then, in a second step, the spectral energy density of the relic gravitons is derived [27] (see also, for instance, [21–23]). The spectral energy density can be also directly assessed by numerical means without passing through the transfer function of the amplitude: this will be the approach followed here. Within the first strategy the power spectrum is given by

$$\mathcal{P}_{\rm T}(k,\tau_0) = \frac{9j_1^2(k\tau_0)}{|k\tau_0|^2}\left[1 + c_1\left(\frac{k}{k_{\rm eq}}\right) + b_1\left(\frac{k}{k_{\rm eq}}\right)^2\right]\bar{\mathcal{P}}_{\rm T}(k), \tag{15}$$

where,[2] according to [21], $c_1 = 1.34$ and $b_1 = 2.50$. In Eq. (15) $j_1(y) = (\sin y/y^2 - \cos y/y)$ is the spherical Bessel function of first kind which is related to the approximate solution of the evolution equations for the tensor mode functions whenever the solutions are computed deep in the matter-dominated phase (i.e. $a(\tau) \simeq \tau^2$). To obtain the spectral energy density, Eq. (11) must then be evaluated in the limit $k^2 \gg \mathcal{H}^2$ (i.e. wavelengths inside the Hubble radius). In the latter limit the tensor mode functions satisfy $|g_k(\tau)| \simeq k f_k(\tau)$ and Eq. (11) then gives:

$$\Omega_{\rm GW}(k,\tau_0) = \frac{k^2}{12\mathcal{H}_0^2}\mathcal{P}_{\rm T}(k,\tau_0),$$
$$\lim_{k\gg k_{\rm eq}}\Omega_{\rm GW}(k,\tau_0) \simeq \frac{3b_1}{8a_0^2H_0^2\tau_0^4k_{\rm eq}^2}\left(\frac{k}{k_{\rm p}}\right)^{n_{\rm T}}. \tag{16}$$

Since $\mathcal{P}_{\rm T}(k,\tau_0)$ oscillates also $\Omega_{\rm GW}(k,\tau_0)$ will oscillate. In the limit $k \gg k_{\rm eq}$ the cosine will dominate the expression of $j_1(k\tau_0)$ and the second result of Eq. (16) arises by replacing $\cos^2(k\tau_0) \to 1/2$. If we take $b_1 = 2.5$ in the second relation of Eq. (16), then $3b_1/8 \equiv 15/16 = 0.9375$. If we take instead our results (i.e. $b_1 = 2.683$) we will get, for the same quantity, 1.006. What appears in Eq. (15) is the transfer function of the tensor amplitude which literally transfers the power spectrum $\bar{\mathcal{P}}_{\rm T}$ inside the Hubble radius.

In a complementary perspective, the consistent numerical solution of Eqs. (5) and (6) allows for a numerical calculation of $\Omega_{\rm GW}(k,\tau)$ according to Eq. (11). Instead of fitting the final result in terms of a putative (semi-analytic) amplitude for the mode function, the momentum (or frequency) profile of the spectral energy density will be obtained directly by numerical methods. As usual, initial conditions for the numerical integration are given for $k\tau \ll 1$. The system is then followed through Hubble crossing (i.e. $k\tau \simeq 1$). Finally, when $k\tau \gg 1$ the expression of $\Delta_\rho(k,\tau)$ can be read-off in the asymptotic regime. In Fig. 1 (plot at the left) the numerical integration across the radiation–matter transition is illustrated. Instead of phrasing the numerical integration in terms of $k$ and $\tau$, it is practical to use $x = k\tau$ and $\kappa = k/k_{\rm eq}$ as preferred variables. To be accurate on the initial conditions a fully analytic solution of Eq. (6), valid across the radiation–matter transition, can be safely employed:

$$a(\tau) = a_{\rm eq}\left[\left(\frac{\tau}{\tau_1}\right)^2 + 2\left(\frac{\tau}{\tau_1}\right)\right],$$
$$\frac{a_0}{a_{\rm eq}} = 1 + z_{\rm eq} = 3195.17\left(\frac{h_0^2\Omega_{\rm M0}}{0.1326}\right)\left(\frac{h_0^2\Omega_{\rm R0}}{4.15\times 10^{-5}}\right)^{-1},$$
$$\tau_{\rm eq} = \bigl(\sqrt{2}-1\bigr)\tau_1 = 120.658\left(\frac{h_0^2\Omega_{\rm M0}}{0.1326}\right)^{-1}\left(\frac{h_0^2\Omega_{\rm R0}}{4.15\times 10^{-5}}\right)^{1/2}\ {\rm Mpc}. \tag{17}$$

In the limit $x \ll 1$ the initial conditions for the mode functions are determined directly (and up to phase factors) from Eq. (13). Since the system is linear, the tensor mode functions can be always rescaled through their initial value; the energy transfer function is therefore defined by the following limit

$$\lim_{x\gg 1}\Delta_\rho(\kappa,x) \equiv T_\rho^2(\kappa)\Delta_\rho(\kappa,x_{\rm i}), \quad x_{\rm i} \ll 1. \tag{18}$$

In Fig. 1 the results of the numerical integration are reported in terms of $\Delta_\rho(\kappa,x)$ for different values of $\kappa$ (see plot at the left). Always in Fig. 1 (plot at the right), $T_\rho^2(\kappa)$ can be computed numerically: the diamonds correspond to the numerical points and the full line (in the plot at the right) is the numerical fit obtained by means of standard methods in the analysis of the regressions:

$$T_\rho(k/k_{\rm eq}) = \sqrt{1 + c_2\left(\frac{k_{\rm eq}}{k}\right) + b_2\left(\frac{k_{\rm eq}}{k}\right)^2},$$
$$c_2 = 0.5238, \quad b_2 = 0.3537. \tag{19}$$

For a successful numerical determination of $T_\rho(\kappa)$ the initial integration variable should be sufficiently small (i.e. $x_{\rm i} = k\tau_{\rm i} \ll 1$) in

[2] By repeating the analysis of [21] we obtained $a_1 = 1.260$ and $b_1 = 2.683$ which is fully compatible with the results of [21]. In the approach of [21] the calculation of the amplitude transfer function, in fact, involve a delicate matching on the phases of the tensor mode functions. Conversely, if the transfer function is computed directly for the spectral energy density, the oscillatory contributions are suppressed as the wavelengths get shorter than the Hubble radius (see below).

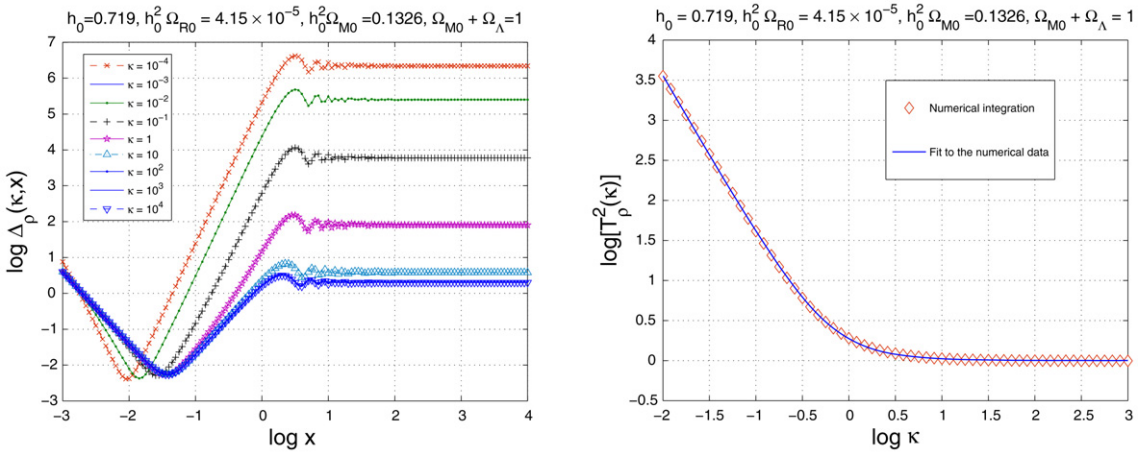


**Fig. 1.** The spectral energy density (see Eq. (11)) is integrated across the radiation matter transition for different values of $\kappa = k/k_{\rm eq}$ (plot at the left). A finer grid in $\kappa$ (plot at the right), allows for the computation of the energy transfer function whose form can be fitted by an appropriate analytical expression (see Eq. (19)).

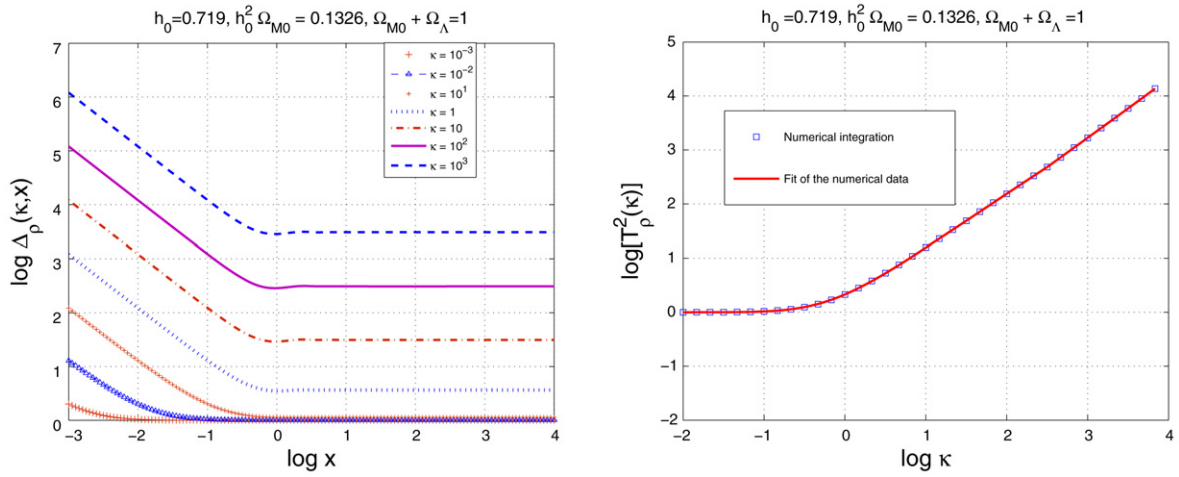


**Fig. 2.** The spectral energy density is integrated across the transition between the stiff epoch and the radiation-dominated epoch for different values of $\kappa$ (plot at the left). Following the same procedure used in the case of Fig. 1 the energy transfer function can be obtained and fitted by the appropriate analytic expression (plot at the right).

such a way that, at the initial time, the mode $k_{\rm eq} = \tau_{\rm eq}^{-1}$ had a corresponding wavelength much smaller than the Hubble radius at $\tau_{\rm i}$. Second, $x_{\rm f}$ should be sufficiently large so that, effectively, $\Delta_\rho(x_{\rm f}, \kappa)$ is constant up to terms $\mathcal{O}(1/x_{\rm f})$ (see also below Eq. (22)). Finally, the grid in $\kappa$ should be sufficiently fine to allow for a reasonable fit. Using Eq. (19), the spectral energy density can be written, in the absence of free streaming, as

$$h_0^2\Omega_{\rm GW}(\nu,\tau_0) = \mathcal{N}_\rho T_\rho^2(\nu/\nu_{\rm eq}) r_{\rm T}\left(\frac{\nu}{\nu_{\rm p}}\right)^{n_{\rm T}} e^{-2\beta\frac{\nu}{\nu_{\rm max}}},$$

$$\mathcal{N}_\rho = 4.165\times 10^{-15}\left(\frac{h_0^2\Omega_{\rm R0}}{4.15\times 10^{-5}}\right), \qquad (20)$$

where $\beta = 6.33$ has been determined numerically assuming a smooth transition between inflation and radiation [28]. Eq. (20), unlike Eqs. (15) and (16), is not strongly oscillating. The rationale for this difference is that, when computing $\Delta_\rho(\kappa, x)$, the oscillating contributions get dynamically suppressed as the wavelengths get shorter than the Hubble radius. A way of understanding this effect is to notice that the crudest approximation for the mode functions in the limit $k\tau \gg 1$ are simple plane waves, i.e.

$$\bar{f}_k(\tau) = \frac{1}{\sqrt{2k}}\left[c_+(k)e^{-ik\tau} + c_-(k)e^{ik\tau}\right],$$

$$\bar{g}_k(\tau) = -i\sqrt{\frac{k}{2}}\left[c_+(k)e^{-ik\tau} - c_-(k)e^{ik\tau}\right]. \qquad (21)$$

Using Eq. (21) into Eq. (11) and enforcing the limit $x \to x_{\rm f} \gg 1$,

$$\Delta_\rho(\kappa, x_{\rm f}) = \kappa\left(\left|c_+(\kappa)\right|^2 + \left|c_-(\kappa)\right|^2\right) + \mathcal{O}\left(\frac{1}{x_{\rm f}}\right), \qquad (22)$$

which proofs that the oscillating contributions are suppressed and that $\Delta_\rho(\kappa, x_{\rm f})$ is proportional to what are called, in the jargon, mixing coefficients. The considerations developed in the case of the radiation–matter transition also apply, for instance, to the stiff-radiation transition. In Fig. 2, for instance, the transition between a radiation-dominated phase and a stiff phase (with $w_{\rm t} = 1$) is illustrated. This time the energy transfer function will be increasing with the wavenumber (see Fig. 2, plot at the right) and the energy transfer function will be given, this time, by

$$T^2(k/k_{\rm s}) = 1.0 + 0.204\left(\frac{k}{k_{\rm s}}\right)^{1/4} - 0.980\left(\frac{k}{k_{\rm s}}\right)^{1/2} + 3.389\left(\frac{k}{k_{\rm s}}\right) - 0.067\left(\frac{k}{k_{\rm s}}\right)\ln^2(k/k_{\rm s}), \qquad (23)$$

where $k_{\rm s} = \tau_{\rm s}^{-1}$ and $\tau_{\rm s}$ the time at which the plasma becomes dominated by radiation. The fact that the spectral energy density increases linearly (up to logarithmic corrections) fits with the analytical results of [14,15] where, however, the slow-roll corrections were neglected. Further details on this approach will be given in a forthcoming paper [28].

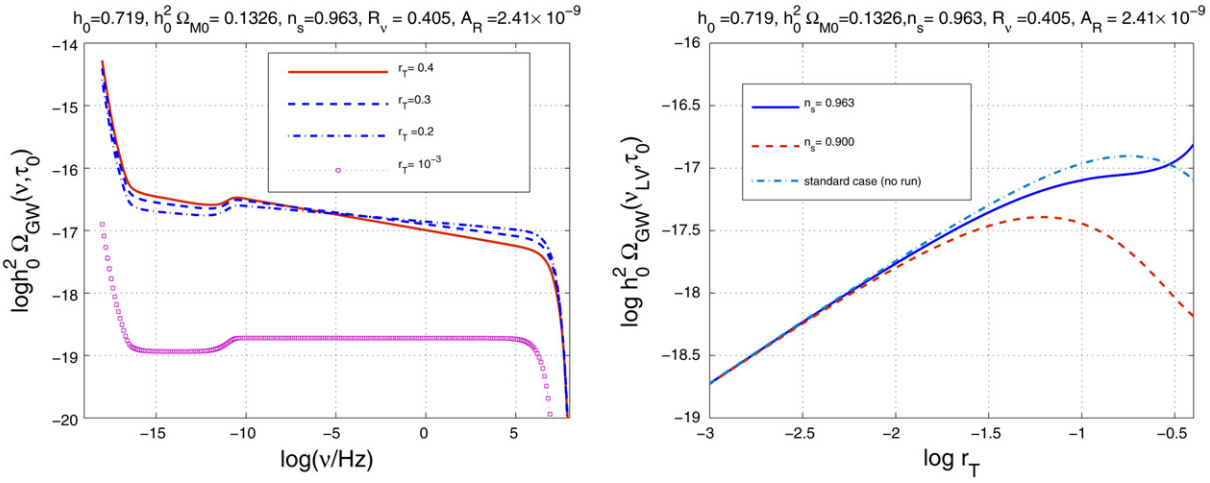


**Fig. 3.** The spectral energy density of the relic gravitons is illustrated in the case of the (conventional) ΛCDM paradigm supplemented by the tensor to scalar ratio $r_{\rm T}$. The parameters are fixed to the best-fit values derived by comparing the ΛCDM paradigm with the WMAP 5-yr alone [1,2].

The outlined computational procedure allows for a reasonably accurate estimate of the spectral energy density of the relic gravitons in a variety of models. In Figs. 3 and 4 the spectral energy density is reported, respectively, in the conventional case and in the TΛCDM scenario taking into account, in both cases, the late-time effects which can marginally reduce the amplitude. Depending upon $R_\nu$ (i.e. the neutrino fraction in the radiation plasma), the tensor amplitude and the spectral energy density get reduced. For three families of massless neutrinos (as implied by the WMAP 5-yr best fits and as assumed in the pivotal ΛCDM paradigm) $R_\nu = 0.405$ and the amount of suppression is, approximately, 0.64 of the value $\Omega_{\rm GW}(\nu,\tau_0)$ has when the very same effect is not taken into account.

The effect of a progressive reduction of relativistic degrees of freedom has been approximately taken into account. In the least favourable case the reduction of the relativistic degrees of freedom is flat in frequency and proportional to $(g_\rho/g_{\rho 0})(g_{\rm s}/g_{\rm s0})^{-4/3}$ where $g_{\rho 0} = 3.36$, $g_{\rm s0} = 3.90$ [21,22]. Note that $g_\rho$ and $g_{\rm s}$ are the relativistic degrees of freedom appearing, respectively, in the energy and in the entropy density. Finally, there is a modification in the spectrum connected with the late dominance of the dark energy [21]. The most prominent effect is independent on the frequency: the spectral energy density is suppressed by an extra-factor, i.e. $(\Omega_{\rm M0}/\Omega_\Lambda)^2$. In the case of the WMAP 5-yr data alone, the ΛCDM paradigm gives $\Omega_\Lambda = 0.742$ and $\Omega_{\rm M0} = 0.258$. Intuitively this means that $\mathcal{N}_\rho$ (appearing in Eq. (20)) is further suppressed by a factor $\mathcal{O}(0.120)$. In Fig. 3 (plot at the left) $h_0^2\Omega_{\rm GW}$ is illustrated as a function of the frequency $\nu = k/(2\pi)$ by taking into account all the late-time effects mentioned above. The pivot frequency $\nu_{\rm p} = 3.092$ aHz corresponds[3] to the pivot wavenumber of Eq. (13). The spectral energy density (see Fig. 1 plot at the left) consists of a decreasing region (at low frequencies) which is followed by a nearly scale-invariant plateau for frequencies $\nu > \nu_{\rm eq}$ where

$$\nu_{\rm eq} = \frac{k_{\rm eq}}{2\pi} = 1.281\times 10^{-17}\biggl(\frac{h_0^2\Omega_{\rm M0}}{0.1326}\biggr)\biggl(\frac{h_0^2\Omega_{\rm R0}}{4.15\times 10^{-5}}\biggr)^{-1/2}\ {\rm Hz}, \quad (24)$$

is the frequency corresponding to matter–radiation equality.[4] The WMAP 5-yr Collaboration [1,2] give an experimental determination of $k_{\rm eq}$ (i.e. $k_{\rm eq} = 0.00999^{+0.00028}_{-0.00027}\ {\rm Mpc}^{-1}$) which is fully compatible with the analytical estimate of Eq. (24). According to Fig. 3, $h_0^2\Omega_{\rm GW}(\nu,\tau_0)$ decreases exponentially for $\nu > \nu_{\rm max}$ where

$$\nu_{\rm max} = 0.346\biggl(\frac{\epsilon}{0.01}\biggr)^{1/4}\biggl(\frac{\mathcal{A}_{\mathcal{R}}}{2.41\times 10^{-9}}\biggr)^{1/4} \times\biggl(\frac{h_0^2\Omega_{\rm R0}}{4.15\times 10^{-5}}\biggr)^{1/4}\ {\rm GHz}. \quad (25)$$

While $\nu_{\rm eq}$ does not depend upon the specific model, $\nu_{\rm max}$ depends, in principle, from the amount of redshift between the end of inflation and the present epoch. The shallow depression arising in the nearly scale-invariant plateau of Fig. 3 (plot at the left) is due to neutrino free streaming and it is present for $\nu_{\rm eq} < \nu < \nu_{\rm bbn}$ where

$$\nu_{\rm bbn} = 2.252\times 10^{-11}\biggl(\frac{N_{\rm eff}}{10.75}\biggr)^{1/4}\biggl(\frac{T_{\rm bbn}}{\rm MeV}\biggr)\biggl(\frac{h_0^2\Omega_{\rm R0}}{4.15\times 10^{-5}}\biggr)^{1/4}\ {\rm Hz} \simeq 0.01\ {\rm nHz}. \quad (26)$$

The frequency band of the terrestrial interferometers [7–10] ranges between few Hz and 10 kHz with a maximum in the sensitivity to a stochastic background[5] for, approximately, $\nu_{\rm LV} \simeq 0.1$ kHz. Since $\nu_{\rm eq} < \nu_{\rm LV} < \nu_{\rm max}$, Fig. 1 implies (plot at the left) that $h_0^2\Omega_{\rm GW}(\nu_{\rm LV},\tau_0) \simeq 10^{-17}$. To be even more quantitative, in Fig. 3 (plot at the right), $h_0^2\Omega_{\rm GW}(\nu_{\rm LV},\tau_0)$ is illustrated as a function of $r_{\rm T}$. In the same plot, the dot-dashed curve refers to the standard case discussed in Eq. (14); the full and dashed curves refer instead to the situation where the spectral index depends upon the frequency as $n_{\rm T} = -r_{\rm T}/8 + (r_{\rm T}/16)[(n_{\rm s}-1) + (r_{\rm T}/8)]\ln(\nu/\nu_{\rm p})$. Fig. 3 shows that, in both situations, $h_0^2\Omega_{\rm GW}(\nu_{\rm LV},\tau_0) \simeq \mathcal{O}10^{-17}$ given the current limits on $r_{\rm T}$.

In the case of an exactly scale invariant spectrum the correlation of the two (coaligned) LIGO detectors with central corner stations in Livingston (Lousiana) and in Hanford (Washington) might reach a sensitivity to a flat spectrum which is [29]

$$h_0^2\Omega_{\rm GW}(\nu_{\rm LV}) \simeq 6.5\times 10^{-11}\biggl(\frac{1\ {\rm yr}}{T}\biggr)^{1/2}{\rm SNR}^2, \quad \nu_{\rm LV} = 0.1\ {\rm kHz}, \quad (27)$$

[3] Whenever needed, the prefixes of the International System of units will be consistently adopted: 1 aHz $= 10^{-18}$ Hz, 1 fHz $= 10^{-15}$ Hz and so on.

[4] In Eq. (24) $\Omega_{\rm M0}$ and $\Omega_{\rm R0}$ are, respectively, the critical fractions of matter and radiation of the putative ΛCDM model.

[5] The sensitivity to a given signal depends upon various factors. For intermediate frequency the signal to noise ratio is also sensitive to the form of the overlap reduction function which depends upon the mutual position and relative orientations of the interferometers. The overlap reduction function effectively cuts-off the integral which defines the signal to noise ratio for a typical frequency $\nu \simeq 1/(2d)$ where $d$ is the separation between the two detectors.

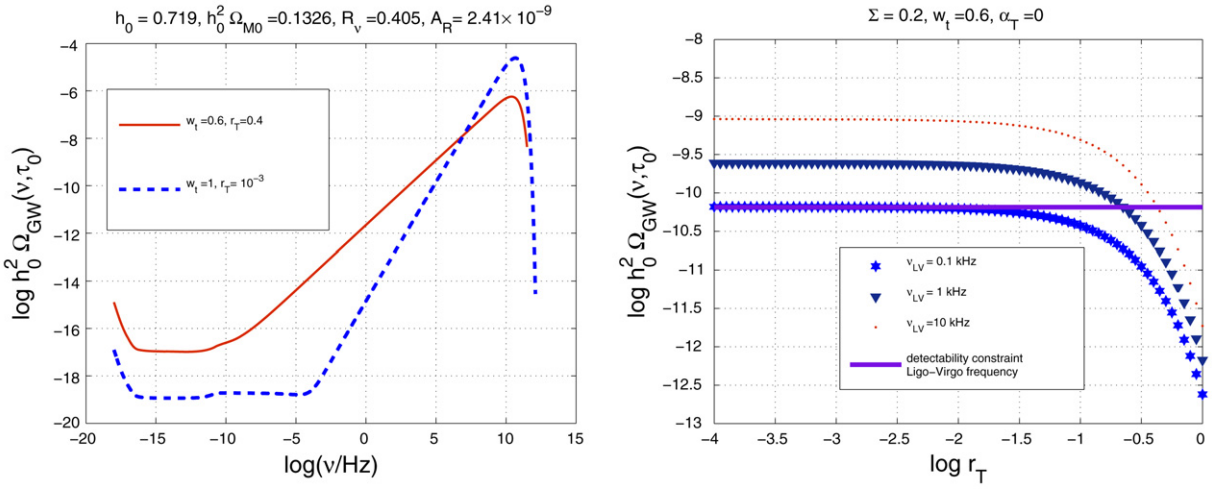


**Fig. 4.** The spectral energy density of the relic gravitons in the case of the TΛCDM scenario. The parameters are fixed to the best-fit values derived by comparing the ΛCDM paradigm with the WMAP 5-yr alone [1,2].

where $T$ denotes the observation time and SNR is the signal to noise ratio. Eq. (27) is in close agreement with the sensitivity of the advanced Ligo apparatus [7] to an exactly scale-invariant spectral energy density [30]. Eq. (27) together with the plots at the right in Fig. 3 suggest that the relic graviton background predicted by the ΛCDM paradigm is not directly observable by wide-band interferometers in their advanced incarnation. The minuteness of $h_0^2\Omega_{\rm GW}(\nu_{\rm LV},\tau_0)$ stems directly from the assumption that the inflationary phase is suddenly followed by the radiation-dominated phase.

Let us then posit that between the end of inflation and the onset of the radiation-dominated phase a sufficiently long stiff phase takes place. In this case the spectral energy density of the relic gravitons will increase for frequencies larger than $\nu_{\rm s} = k_{\rm s}/(2\pi)$. Assuming that the inflationary phase is be of quasi-de Sitter type and characterized by a given value of $r_{\rm T}$, it must always happen, no matter how the parameters of the model are assigned, that $\nu_{\rm s} > \nu_{\rm bbn}$.

The frequency scale $\nu_{\rm s}$ is related to the duration of the stiff phase and it is bounded from below by the nucleosynthesis frequency. The slope of the spectral energy density in the high-frequency branch is related, ultimately, to the sound speed and it is bounded, from above, by the speed of light. These are the two supplementary parameters of TΛCDM scenario. In Fig. 4 (see plot at the left) the spectral energy density computed in the TΛCDM scenario is illustrated for two different values of $w_{\rm t}$ and $r_{\rm T}$. For $\nu > \nu_{\rm s}$ the spectral energy density acquires a blue spectrum.[6]

Defining as $H \simeq (\epsilon\pi\mathcal{A}_{\mathcal{R}})^{1/2} M_{\rm P}$ the typical inflationary curvature scale and as $H_{\rm r}$ the Hubble rate at the onset of the radiation epoch, $\nu_{\rm s}$ and $\nu_{\rm max}$ can be written, in the TΛCDM scenario, as

$$\nu_{\rm s} = 1.177\times 10^{11}\,\Sigma^{\gamma}(\pi\epsilon\mathcal{P}_{\mathcal{R}})^{\frac{\gamma+1}{4}}\left(\frac{h_0^2\Omega_{\rm R0}}{4.15\times 10^{-5}}\right)^{1/4}\ {\rm Hz}, \tag{28}$$

$$\nu_{\rm max} = 1.177\times 10^{11}\,\Sigma^{-1}\left(\frac{h_0^2\Omega_{\rm R0}}{4.15\times 10^{-5}}\right)^{1/4}\ {\rm Hz},$$

$$\Sigma = \left(\frac{H}{M_{\rm P}}\right)^{\frac{\gamma+1}{2\gamma}}\left(\frac{H_{\rm r}}{M_{\rm P}}\right)^{\frac{1}{2\gamma}}, \tag{29}$$

where $\gamma \equiv \gamma(w_{\rm t}) = 3(w_{\rm t}+1)/(3w_{\rm t}-1)$. By definition $\Sigma$ is fully determined by fixing $H_{\rm r}$. So, $\Sigma$ and $\gamma(w_{\rm t})$ can be chosen as the two pivotal parameters of the TΛCDM scenario. Equivalently $\Sigma$ and $\gamma$ can be traded for $\nu_{\rm s}$ and for the slope of the spectral energy density during the stiff phase (which is given, up to logarithmic corrections) by $(6w_{\rm t}-2)/[(3w_{\rm t}+1)]$. As stressed above, the natural upper limit for the spectral slope is exactly 1 which is the maximally stiff fluid compatible with causality [19].

The frequency $\nu_{\rm s}$ can be much larger than $\nu_{\rm bbn}$ (for instance $\nu \simeq$ mHz in [15]) but cannot be smaller than $\nu_{\rm bbn}$ which constitutes a natural lower limit for $\nu_{\rm s}$. If $\nu_{\rm s} < \nu_{\rm bbn}$ the plasma would be stiff also throughout nucleosynthesis which is unacceptable. The observed abundances of the light elements (together with CMB data) also constrain the total energy density of the relic gravitons, i.e. the integral of $\Omega_{\rm GW}(\nu,\tau_0)$ over the frequency. This bound is usually expressed as[7]:

$$h_0^2\Omega_{\rm GW}(\tau_0) = h_0^2\int_{\nu_{\rm bbn}}^{\nu_{\rm max}}\Omega_{\rm GW}(\nu,\tau_0)\,d\ln\nu$$
$$= 5.6\times 10^{-6}\left(\frac{h_0^2\Omega_{\gamma 0}}{2.47\times 10^{-5}}\right)\Delta N_\nu \tag{30}$$

where $\Delta N_\nu$ is the equivalent number of extra-relativistic species at the onset of standard big-bang nucleosynthesis.[8] In the standard scenario for the synthesis of light nuclei, $0.2 < \Delta N_\nu < 1$, and therefore $h_0^2\Omega_{\rm GW}(\tau_0)$ will be constrained accordingly. In Fig. 2 (plot at the right) the spectral energy density is reported as function of $r_{\rm T}$ in the context of the TΛCDM scenario and for typical frequencies in the operating window of wide-band interferometers. As $r_{\rm T}$ diminishes, the amplitude of the spectral energy density is almost constant. The latter occurrence arises for two independent reasons. On one hand the most relevant constraint, in the case of growing spectral energy densities, is the one provided by Eq. (8) and enforced in both plots of Fig. 2. On the other hand, the frequency $\nu_{\rm s}$ depends also upon $r_{\rm T}$ (through $\epsilon$, see Eqs. (14) and (29)). It should be finally appreciated, from Figs. 2 and 3,

[6] The spectrum is blue, in general terms, if it is increasing with frequency. The slow-roll dynamics always implies, within the ΛCDM scenario, much milder scaling violations which involve only red spectra, i.e. spectra which are very slowly decreasing in frequency like those of Fig. 1 (see plot at the left).

[7] Coherently with established conventions ln will denote the natural logarithm, while the logarithms to base 10 (i.e. common logarithms) will be denoted by log.

[8] The language of Eq. (30) may seem a bit contrived but it is a simple consequence of the historical development of the field. The extra-relativistic species were associated, in the past, with families of neutrinos. The nature of the bound on $\Delta N_\nu$ (and hence on $h_0^2\Omega_{\rm GW}(\tau_0)$) does not change if the relativistic species are bosonic (like in the case of gravitons). For a discussion of the derivation of Eq. (8) see [31].

that the pulsar timing bounds (recently revisited [32]) still imply that $h_0^2\Omega_{\rm GW}(\nu_{\rm pulsar},\tau_0) < 1.9\times 10^{-8}$ for a $\nu_{\rm pulsar}\simeq 10$ nHz which is roughly comparable with the inverse of the observation time along which the pulsars timing has been monitored. Such a bound is not constraining for the T$\Lambda$CDM model. The proof goes as follows. Assuming the maximal growth of the spectral energy density (i.e. that $h_0^2\Omega_{\rm GW}(\nu,\tau_0)\propto\nu$) and the minimal value of $\nu_{\rm s}$ (i.e. $\nu>\nu_{\rm bbn}$), we will have that, at the frequency scale of the pulsars, $h_0^2\Omega_{\rm GW}(\nu_{\rm pulsar},\tau_0)\simeq 10^{-13}$ or even $10^{-14}$ depending upon $r_{\rm T}$. But this value is always much smaller than the constraint stemming from pulsar timing measurements.

In this Letter it has been suggested that the $\Lambda$CDM parameter can be complemented by adding a post-inflationary phase characterized by a sound speed larger than the one of an ultra-relativistic plasma (i.e. $1/\sqrt{3}$). Causality constrains the maximal barotropic index and the maximal sound speed. Big bang nucleosynthesis sets limits both on the maximal duration of the stiff phase and on the total energy density of the relic gravitons. Two new parameters will then be added to the $\Lambda$CDM paradigm which has been dubbed, throughout the Letter, as tensor-$\Lambda$CDM (T$\Lambda$CDM) paradigm since relic gravitons are copiously produced at high frequencies (i.e. larger than 0.1 nHz). The new pivot frequency defines the scale at which the spectral energy density of the relic gravitons starts increasing with a slope which is dictated by the stiff barotropic index. In the T$\Lambda$CDM scenario, which may be seen as an improved version of the models proposed in [14,15], the spectral energy density of the relic gravitons can even be from 6 to 7 orders of magnitude larger than in conventional inflationary models. Along a more technical perspective, a numerical recipe for the calculation of the spectral energy density has been presented.

The advanced versions of wide-band interferometers are germane to the theme of the present investigation. At the moment the CMB data [1,2], large-scale structure observations [3,4] and supernovae light curves [5,6] are used in combined analysis to put bounds on $r_{\rm T}$, i.e. the tensor to scalar ratio. Few years from now the three aforementioned cosmological data sets will still be used to constrain (and hopefully determine) $r_{\rm T}$ while, given the foreseen sensitivities, the (terrestrial) wide-band interferometers will still be unable to set concurrent limits to backgrounds of relic gravitons. Provided the claimed sensitivities will be reached in due time, the considerations presented here give a concrete opportunity of using interferometers data together with the more classic cosmological data sets to rule out (or, more optimistically, rule in) a class of specific models. It is productive to stress that, in the present context, any potential upper limit from wide-band interferometers will directly constrain the post-inflationary thermal history. Cosmology is not tested in a laboratory: therefore the nature of the observations is inextricably bound to the models employed to analyze the data and to the potential redundancy of different data sets. It has been shown here that by complementing a known model with supplementary physical considerations, the three established cosmological data sets can also profit of a qualitatively new class of observations, such as the ones provided by wide-band interferometers. It is tempting to speculate that the perspective of the present Letter could provoke a useful synergy between communities scrutinizing different branches of the graviton spectrum. The fruitful dialogue between the experiments sensitive to small (i.e. $\nu_{\rm p}\simeq$ aHz) and to intermediate frequencies (i.e. $\nu_{\rm LV}\simeq 0.1$ kHz) could be extended, in principle, also to conceptually different kinds of detectors such as microwave cavities [33] and waveguides [34].

## Acknowledgement

It is a pleasure to acknowledge interesting discussions with E. Picasso.

## References

[1] G. Hinshaw, et al., WMAP Collaboration, arXiv: 0803.0732 [astro-ph];
J. Dunkley, et al., WMAP Collaboration, arXiv: 0803.0586 [astro-ph].
[2] B. Gold, et al., WMAP Collaboration, arXiv: 0803.0715 [astro-ph];
E. Komatsu, et al., WMAP Collaboration, arXiv: 0803.0547 [astro-ph];
M. Nolta, et al., WMAP Collaboration, arXiv: 0803.0593 [astro-ph].
[3] W.L. Freedman, et al., Astrophys. J. 553 (2001) 47;
S. Cole, et al., 2dFGRS Collaboration, Mon. Not. R. Astron. Soc. 362 (2005) 505.
[4] D.J. Eisenstein, et al., SDSS Collaboration, Astrophys. J. 633 (2005) 560;
M. Tegmark, et al., SDSS Collaboration, Astrophys. J. 606 (2004) 702.
[5] P. Astier, et al., SNLS Collaboration, Astron. Astrophys. 447 (2006) 31.
[6] A.G. Riess, et al., Supernova Search Team Collaboration, Astrophys. J. 607 (2004) 665;
B.J. Barris, et al., Astrophys. J. 602 (2004) 571.
[7] A. Abramovici, et al., Science 256 (1992) 325;
http://www.ligo.org.
[8] B. Caron, et al., Class. Quantum Grav. 14 (1997) 1461;
http://www.virgo.infn.it.
[9] M. Ando, et al., Phys. Rev. Lett. 86 (2001) 3950;
http://tamago.mtk.nao.ac.jp.
[10] H. Lück, et al., Class. Quantum Grav. 14 (1997) 1471;
http://www.geo600.uni-hannover.de.
[11] B. Abbott, et al., ALLEGRO Collaboration and LIGO Scientific Collaboration, Phys. Rev. D 76 (2007) 022001;
G. Cella, et al., Class. Quantum Grav. 24 (2007) S639;
L. Baggio, et al., AURIGA Collaboration, Class. Quantum Grav. 25 (2008) 095004.
[12] M. Giovannini, Int. J. Mod. Phys. D 13 (2004) 391.
[13] A.R. Liddle, S.M. Leach, Phys. Rev. D 68 (2003) 103503.
[14] M. Giovannini, Phys. Rev. D 58 (1998) 083504.
[15] M. Giovannini, Class. Quantum Grav. 16 (1999) 2905;
M. Giovannini, Phys. Rev. D 60 (1999) 123511.
[16] Y.B. Zeldovich, Mon. Not. R. Astron. Soc. 160 (1972) 1P.
[17] P.J.E. Peebles, A. Vilenkin, Phys. Rev. D 59 (1999) 063505.
[18] V. Sahni, M. Sami, T. Souradeep, Phys. Rev. D 65 (2002) 023518;
H. Tashiro, T. Chiba, M. Sasaki, Class. Quantum Grav. 21 (2004) 1761;
T.J. Battefeld, D.A. Easson, Phys. Rev. D 70 (2004) 103516.
[19] G. Ellis, R. Maartens, M.A.H. MacCallum, Gen. Relativ. Gravit. 39 (2007) 1651.
[20] S. Weinberg, Phys. Rev. D 69 (2004) 023503;
D.A. Dicus, W.W. Repko, Phys. Rev. D 72 (2005) 088302.
[21] W. Zhao, Y. Zhang, Phys. Rev. D 74 (2006) 043503;
Y. Zhang, W. Zhao, T. Xia, Y. Yuan, Phys. Rev. D 74 (2006) 083006.
[22] Y. Watanabe, E. Komatsu, Phys. Rev. D 73 (2006) 123515.
[23] S. Chongchitnan, G. Efstathiou, Phys. Rev. D 73 (2006) 083511;
S. Chongchitnan, G. Efstathiou, Prog. Theor. Phys. Suppl. 163 (2006) 204.
[24] L.H. Ford, L. Parker, Phys. Rev. D 16 (1977) 1601;
L.H. Ford, L. Parker, Phys. Rev. D 16 (1977) 245.
[25] R. Isaacson, Phys. Rev. 166 (1968) 1263;
R. Isaacson, Phys. Rev. 166 (1968) 1272.
[26] M. Giovannini, Phys. Rev. D 73 (2006) 083505;
L. Abramo, Phys. Rev. D 60 (1999) 064004.
[27] M.S. Turner, M.J. White, J.E. Lidsey, Phys. Rev. D 48 (1993) 4613.
[28] M. Giovannini, arXiv: 0807.4317 [astro-ph].
[29] D. Babusci, M. Giovannini, Phys. Rev. D 60 (1999) 083511;
D. Babusci, M. Giovannini, Class. Quantum Grav. 17 (2000) 2621;
D. Babusci, M. Giovannini, Int. J. Mod. Phys. D 10 (2001) 477.
[30] B. Allen, J.D. Romano, Phys. Rev. D 59 (1999) 102001.
[31] M. Giovannini, H. Kurki-Suonio, E. Sihvola, Phys. Rev. D 66 (2002) 043504.
[32] F.A. Jenet, et al., Astrophys. J. 653 (2006) 1571, astro-ph/0609013.
[33] F. Pegoraro, L.A. Radicati, Ph. Bernard, E. Picasso, Phys. Lett. A 68 (1978) 165;
Ph. Bernard, G. Gemme, R. Parodi, E. Picasso, Rev. Sci. Instrum. 72 (2001) 2428;
R. Ballantini, P. Bernard, A. Chincarini, G. Gemme, R. Parodi, E. Picasso, Class. Quantum Grav. 21 (2004) S1241.
[34] A.M. Cruise, Class. Quantum Grav. 17 (2000) 2525;
A.M. Cruise, R.M. Ingley, Class. Quantum Grav. 23 (2006) 6185;
F.Y. Li, M.X. Tang, D.P. Shi, Phys. Rev. D 67 (2003) 104008.